Materials and Design 195 (2020) 109032

Contents lists available at ScienceDirect

Materials and Design

journal homepage: www.elsevier.com/locate/matdes

A method for 3D printing bio-cemented spatial structures using sand and urease active calcium carbonate powder

Christoph Nething [a], Maya Smirnova [a,*], Janosch A.D. Gröning [b], Walter Haase [a], Andreas Stolz [b], Werner Sobek [a]

[a] Institute for Lightweight Structures and Conceptual Design, University of Stuttgart, Pfaffenwaldring 14, 70569 Stuttgart, Germany
[b] Institute for Microbiology, University of Stuttgart, Allmandring 31, 70569 Stuttgart, Germany

HIGHLIGHTS

- Lyophilized urease active calcium carbonate powder facilitates fixation of bacteria in sand during cementation.
- Spatial structures cemented using urease active calcium carbonate powder demonstrate sharply defined boundaries.
- Non-cementable channels facilitate the penetration of the cementation solution into the depth of a 3D printed volume.
- Bio-cemented cylindrical samples (d = 20 mm, h = 20 mm) demonstrate compressive strengths of up to 23 MPa.
- Lyophilized urease active calcium carbonate powder retains 83 % of its initial activity after 6 months storage at -20 °C.

GRAPHICAL ABSTRACT

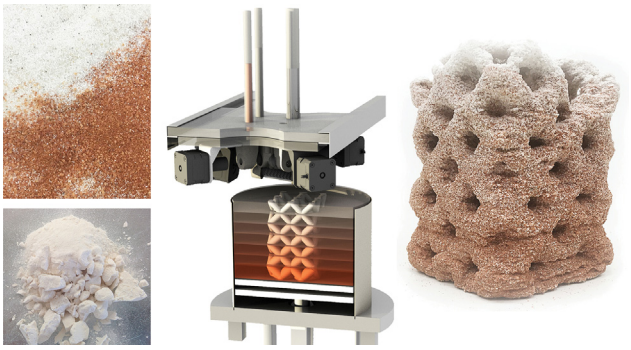

ARTICLE INFO

Article history:
Received 11 April 2020
Received in revised form 30 July 2020
Accepted 1 August 2020
Available online 05 August 2020

Keywords:
Microbially induced calcite precipitation (MICP)
Bio-cement
Additive manufacturing
Biomaterials
Sustainability

ABSTRACT

The substitution of Portland cement with microbially based bio-cement for the production of construction materials is an emerging sustainable technology. Bio-cemented building components such as bricks have been fabricated in molds, where bacteria-containing aggregates solidify when treated with a cementation solution. This restricts component size due to the limited fluid penetration depth and narrows options for component customization. The use of additive manufacturing technologies has the potential to overcome those limitations and to expand the range of bio-cement applications. In the present work an automated process for the production of spatial structures has been developed, in which sand and urease active calcium carbonate powder were selectively deposited within a print volume and treated with a cementation solution. This method provided conditions for calcite precipitation in the powder-containing areas, whereas areas of pure sand served as removable support structure allowing improved fluid exchange. The 3D printed structure was geometrically stable and had sharply defined boundaries. Compressive strength tests on cylindrical specimens showed that the used powder-sand mix was suitable for the production of high-strength bio-cemented material. The present work demonstrates an application of bio-cement in an additive manufacturing process, that can potentially be used to produce resource efficient sustainable building components.

1. Introduction

Since its discovery Portland cement has been of great importance for the building industry, as it allowed the production of durable building

* Corresponding author.
E-mail address: maiia.smirnova@ilek.uni-stuttgart.de (M. Smirnova).

https://doi.org/10.1016/j.matdes.2020.109032

components in a broad variety of forms. The unique binding properties of cement are however associated with up to 8% of the global CO_2 emissions, which originate from two equally contributing sources: process-immanent chemical reactions and the combustion of fossil fuels during cement production [1,2].

Advances in geotechnical and material research have led to the investigation of more sustainable binders. Bio-cementation based on microbially induced calcite precipitation (MICP) is a promising biomediated technique [3], in which sand grains are bound together by the formation of calcium carbonate crystals. One form of MICP is the crystallization through microbial urea hydrolysis from a solution containing urea and calcium ions [4,5]. *Sporosarcina pasteurii* is a non-pathogenic bacterial species, which is frequently used in the MICP process due to its high urease activity [6–8].

MICP has been investigated for the production of building components such as bricks [9,10] and beams [11]. Samples are produced in a two-step process, in which sand-filled molds are inoculated with bacterial suspensions and then are either repeatedly flushed with or fully immersed in a cementation solution containing calcium ions and urea (percolation [12] or immersion [13,14] methods).

The insufficient penetration of chemicals into the depth of the components can result in inhomogeneous cementation. This can be caused by clogging of the pore volumes close to the injection point [15] or by the depletion of urea or calcium ions in the layers that first come into contact with the cementation solution [16]. Since the mechanical strength is related to the degree of calcium carbonate precipitation [17,18], eliminating the poorly cemented areas is essential for the production of large-scale high-strength building components.

A mathematical model validated by experimental studies demonstrates that the cementation depth can be increased by increasing the infiltration rate of the cementation solution or by reducing the in-situ urease activity of the sample [15]. Although this leads to the more even distribution of calcium carbonate crystals throughout the sample volume, the amount of calcium carbonate, precipitated close to the surface, decreases. This implies, that the potential maximum mechanical strength is not fully exploited.

The overall cementation level can be increased without affecting the cementation depth by increasing the surface exposed to the cementation solution for example by using full contact molds (FCM) [19]. However, studies on a beam cemented in an FCM still demonstrated 40–67% difference in calcium carbonate content between samples taken from the inside and samples taken close to the surface of the beam [11].

A method to improve penetration, proposed in this study, is based on the creation of non-cementable channels of pure sand within the otherwise bacteria-containing sand volume. The channels allow the cementation solution to penetrate into the depth of the component without the chemicals being depleted. This creates conditions for calcium carbonate precipitation in the bacteria-containing areas. The pure sand also encloses the component and serves as a removable scaffold.

When designing spatial components with channels, a proper fluid circulation and exchange must be considered alongside with the load-bearing performance. The use of formworks makes it difficult to achieve the necessary degree of customization to fulfill both requirements. Therefore, an automated 3D printing process has been developed in this study to expand the range of applications of bio-cement.

In the case of non-cementable channels, microbial transport in a saturated porous media [20] can cause bacteria to move into the areas of pure sand. Since the precipitation of calcium carbonate crystals occurs around bacterial cells [21], the contamination of the channels of pure sand with bacteria would lead to their cementation. Different immobilization techniques were developed to restrain bacteria in sand during the treatment with cementation solution [22,23]. One of the promising approaches is based on premixing sand with an urease active bioslurry, which contains calcium carbonate crystals precipitated around bacterial cells [24]. In the present study the bioslurry has been modified to a urease active calcium carbonate powder, which due to its dry consistency allowed the precise material deposition in a 3D printing process.

2. Materials and methods

2.1. Cultivation of Sporosarcina pasteurii

Sporosarcina pasteurii (strain DSM 33) was obtained from the German Collection of Microorganisms and Cell-Cultures GmbH (DSMZ). The strain was inoculated from an agar plate into 10 ml DSMZ medium 220 (15 g peptone from casein, 5 g peptone from soymeal, 5 g NaCl and 20 g urea per 1000 ml at a pH of 8.2) at 30 °C under constant shaking (100 rpm). After 72 h 200 ml of DSMZ medium 220 were inoculated with this liquid culture and the preculture incubated under the same conditions for further 24 h. Then, 8 l of double concentrated DSMZ 220 medium (30 g peptone from casein, 10 g peptone from soymeal, 5 g NaCl, 20 g urea per liter) were inoculated with the pre-culture. The bacteria were grown at 30 °C in an aerated fermenter using a stirrer speed of 600 rpm. After 48 h the bacterial culture reached an optical density (OD 546 nm) of about 4.8.

2.2. Preparation of the urease active calcium carbonate powder

The bioslurry (Fig. 1 a) was prepared following a slight modification of the method developed by Cheng & Shahin [24]. The pH of the bacterial culture was lowered to 7.9 by adding 85% (*v*/v) H_3PO_4. Several portions of $CaCl_2$ x 2 H_2O (final concentration 0.4 M) and urea (final concentration 0.4 M) were added to the bacterial culture to induce calcium carbonate precipitation. The resulting suspension was stirred (600 rpm) in a fermenter for about 6 h at room temperature. Subsequently, the suspension was left without stirring for 14 h to allow the precipitated material to settle to the bottom of the fermenter. The supernatant was then poured off and the precipitate was dried on a folded filter using a Büchner funnel in combination with a vacuum pump. The resulting bioslurry was lyophilized in a freeze-dryer (Christ Alpha-I5) to achieve the powder-consistency (Fig. 1 b). Thus, about 500 g of the urease active calcium carbonate powder were prepared from 8 l of bacterial culture. The powder was then vacuum-sealed and stored at −20 °C (Fig. 1 c).

Fig. 1. Stages of calcium carbonate powder preparation: (a) Bioslurry before lyophilization; (b) Urease active calcium carbonate powder after lyophilization; (c) Vacuum-sealed powder.

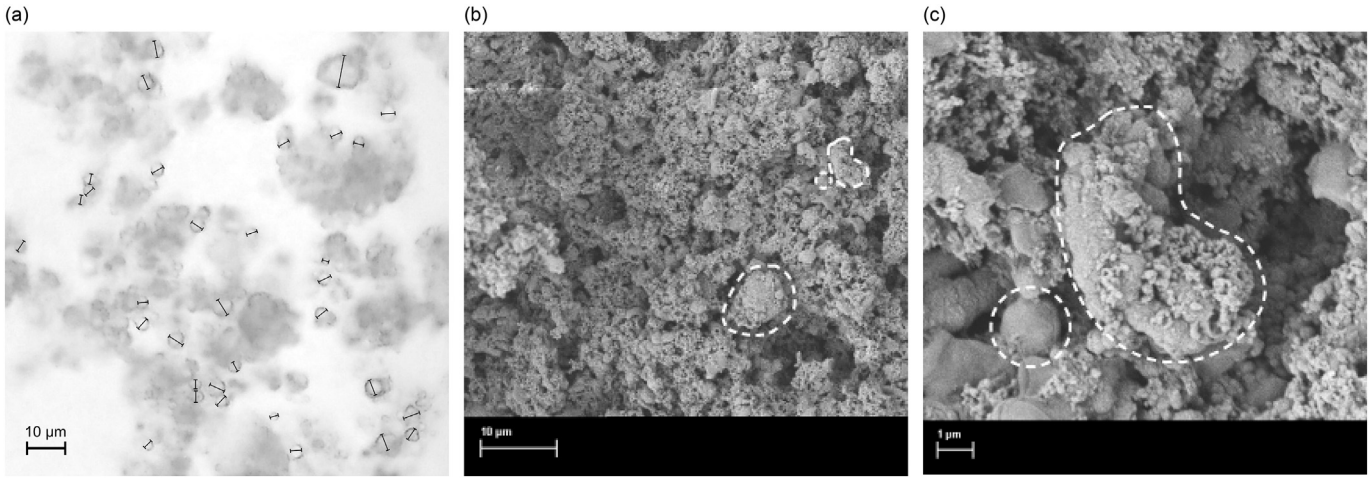

Fig. 2. Particle size determination of the urease active calcium carbonate powder by: (a) Optical microscopy (magnification 400 x); (b, c) Scanning electron microscopy (SEM).

The size of the calcium carbonate particles in the urease active calcium carbonate powder was determined by optical microscopy (magnification 400 x) and ranged from 1.3 µm to 8 µm (Fig. 2a). This was validated by the images taken with the scanning electron microscope (SEM) (Fig. 2b and c). SEM-images show, that the particles are covered with even smaller crystals of 0.1 µm.

2.3. Urease activity of the powder

The urease activity of the powder was determined by measuring the release of ammonia from urea according to the method described by Black et al. [25]. 4.4 g of powder were suspended and washed in 40 ml of H_2O. 262.3 mg of the wet powder were resuspended in 1 ml of H_2O and diluted with H_2O to reach a powder concentration of 1.3 mg/ml. The urea solution (60 µl, 100 mM) was added to 540 µl of powder suspension (540 µl) and placed on a shaker. Samples (60 µl) were taken every 10 min (5 samples in total) and centrifuged. The supernatant was then used for the ammonium measurement.

2.4. Influence of the cementation conditions on the depth and compressive strength of bio-cemented cylindrical samples

2.4.1. Samples preparation

Silica sand (grain size 63–250 µm, Holcim Kies und Beton GmbH, Germany) was premixed with the urease active calcium carbonate powder (0.4% - 5% (*w*/w)). The mixes were moistened with 3 ml of the cementation solution with the same concentration as the cementation solution used for the subsequent treatment. The moistened powder-sand mixes were then compacted in layers of 5 mm into 20 ml plastic syringe bodies (d = 20 mm) equipped with a filter paper at the bottom. Each layer was compressed with a slightly trimmed syringe plunger. A layer of coarse sand (5 mm, 600–800 µm, Holcim Kies und Beton GmbH, Germany) was placed on top of the powder-sand column to prevent erosion by the inflowing cementation solution (Fig. 3). The columns were fed with 5 ml of cementation solution (500, 750 or 1000 mM $CaCl_2$ and urea) with pH 6 to 7 at temperatures of 4 °C, 10 °C or 22 °C every 4 h. The supply of the cementation solutions into the syringe bodies was automated by valves connected to a microcontroller (Arduino Mega). The pH value of the outflowing solutions ranged from 8.5 to 9.5. The treatment was applied for 3 to 5 days until the flow through the syringes stopped or the pH value of the outflowing solution was equal to that of the inflowing solution, indicating that bacterial activity had ceased. Subsequently, the cemented cylindrical specimens were removed from the syringe bodies, rinsed with deionized water and allowed to dry at 60 °C for 24 h.

The tested combinations with different concentrations of cementation solutions and powder contents at specific temperatures are summarized in Table 1.

2.4.2. Cementation depth

The cementation depth was determined by measuring the distance between the highest and the lowest points that displayed a fully cemented cross section (Fig. 4).

Fig. 3. Preparation of bio-cemented cylindrical samples: (a) Dry urease active calcium carbonate powder and sand; (b) Powder-sand mix moistened with the cementation solution; (c) Syringe bodies filled with the powder-sand mix during the treatment with cementation solutions.

Table 1
The tested combinations with different concentrations of cementation solutions and powder contents at specific temperatures.

Concentration of the cementation solution, mM	Powder content % (w/w) at		
	4 °C	10 °C	22 °C
500	–	1.6, 2.4	–
750	1.5, 5.0	0.4, 0.8, 1.2, 1.6, 2.0, 2.4, 2.8	1.5, 5.0
1000	–	1.6, 2.4	–

2.4.3. Unconfined compressive strength (UCS)

The unconfined compressive strength of the cylindrical samples was measured based on the testing standard DIN EN 1926:2006 for natural stone [26] with a path - controlled application of the axial load at a constant rate of 0.5 mm/min and sample dimensions of 20 mm (diameter to height ratio of 1:1). The tests were conducted on the testing machine SP-SRG 5000 and the testing frame ZDEM 20 / 600 (Walter + Bai AG, Switzerland) using the software Proteus MT (FORM + TEST Seidner & Co. GmbH, Germany).

2.5. Initial experiments: Cementation of the urease active calcium carbonate powder-sand mix surrounded by pure sand

Silica sand with the grain size 63–250 μm was obtained from Holcim Kies und Beton GmbH, Germany. The cementation solution contained 750 mM $CaCl_2$ and 750 mM urea.

A cross-shaped mold was placed on the bottom of a container with an inlet and an outlet port (Fig. 5 a). The inside of the mold was filled with the urease active calcium carbonate powder-sand mix with a powder content of 5% (*w*/w). The surrounding volume of the container was filled with pure sand (Fig. 5 b). The mold was then carefully removed leaving the molded shape in direct contact with the surrounding pure sand. The container was then filled with the cementation solution via the inlet port. The volume was kept saturated for 30 s, then the cementation solution was drained via the outlet port. This treatment was repeated every 4 h for 3 days (Fig. 5 c). Afterwards the pure sand was removed by rinsing with water, leaving the solidified structure (Fig. 5 d).

2.6. Additive manufacturing process

2.6.1. Sand, urease active calcium carbonate powder and cementation solution

Sands of two different colors were used to create the material gradation in the 3D printed structure: fine grain white desert sand (Terrano Wüstensand weiß, Dohse Aquaristik GmbH & Co. KG) and red desert sand (Terrano Wüstensand rot, Dohse Aquaristik GmbH & Co. KG). The grain size of the white sand was determined to be 63–350 μm and of the red sand to be 63–400 μm. The urease active calcium carbonate powder was prepared as described in 2.2. The cementation solution contained 750 mM $CaCl_2$ and 750 mM urea.

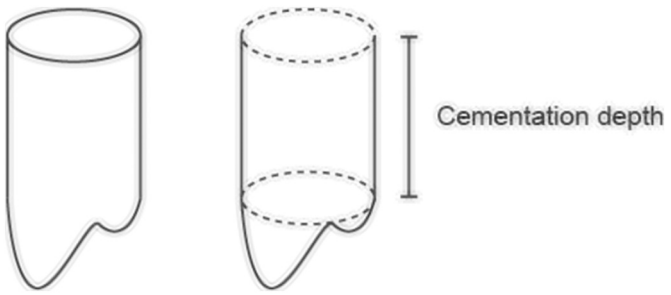

Fig. 4. Measurement of cementation depth.

2.6.2. CNC processing

The mechanical assembly of the 3D printer consisted of a print head moving in the horizontal plane and a print bed with a platform moving in the vertical direction (Fig. 7 a, b). To enable movement the print head was mounted on a CNC-controlled portal milling machine (PFH 3015 G, BZT Maschinenbau GmbH, Germany) and the print bed was equipped with a linear actuator. Both the print head and the print bed were connected to a microcontroller (Arduino Mega). The working instructions were written in a G-Code file, which was then processed by CNC-control software (Eding CNC B.V., The Netherlands), sent to the CNC-CPU and from there to the microcontroller (Fig. 6).

2.6.3. Print head and material flow control

The material supply system of the print head consisted of vertical tubular glass reservoirs, horizontal feed screws, a mixing screw and a deposition nozzle with a diameter of 4.5 mm (Fig. 7 c, d).

The body of the print head as well as the supplying screws and the mixing screw were 3D printed in polyamide via selective laser sintering. To reduce friction and to allow a visual observation of the material transport, glass tubes were used for the print head in the areas of the screws. All the screws were powered by NEMA 17 stepper motors with 1.7 A and 0.59 Nm and were controlled by the microcontroller via A4988 motor drivers.

Sand and urease active calcium carbonate powder were supplied from the glass reservoirs via the feed screws to the mixing screw, where they were combined and further transported to the deposition nozzle. The mixing ratios and volumetric flow rates were regulated by manipulating the rotation speed of the screws. The length and shape of the mixing screw was adjusted to achieve a homogeneous mix. To avoid demixing due to the falling of the powder-sand mix from the output of the mixing screw onto the print plane, the deposition nozzle was installed close to the mixing screw output.

2.6.4. Print bed and cementation solution supply

The print bed consisted of a platform that was moved in the vertical direction inside a plastic cylinder (d = 20 cm, h = 20 cm) by a linear actuator (DSZY 1–12–40-200-POT-IP65, Drive-System Europe) (Fig. 7 e). The linear actuator was controlled via a motor controller (Jrk21v3, Pololu Corporation) and a microcontroller. The cylinder was glued to a base plate with openings for the motor and fastening screws.

The cementation solution was supplied and drained by an inlet and an outlet solenoid valve, attached to the platform. To ensure water tightness the platform needed to be moved to the bottom of the cylinder where it was pressed against the bottom plate and an attached rubber gasket by tightening the screws. Two platinum wires were used as a water sensor to avoid overflowing by connecting one wire to a 5 V pin and the other wire to an analog input pin of the microcontroller.

3. Results

3.1. Characteristics of the urease active calcium carbonate powder

The urease activity of the calcium carbonate powder after lyophilization was measured to be 0.18 μmol/min/mg powder. After six months of storage in a vacuum sealed bag at a temperature of −20 °C the urease activity had declined to 0.15 μmol/min/mg powder and the powder became more clumpy, presumably because it had absorbed water from the air when the bag was shortly unsealed to extract portions of powder to conduct the experiments.

3.2. Influence of the cementation conditions on the depth and compressive strength of bio-cemented cylindrical samples

To investigate the optimal conditions for the production of high-strength deeply cemented material, the samples were produced at different temperatures with different content of the urease active calcium

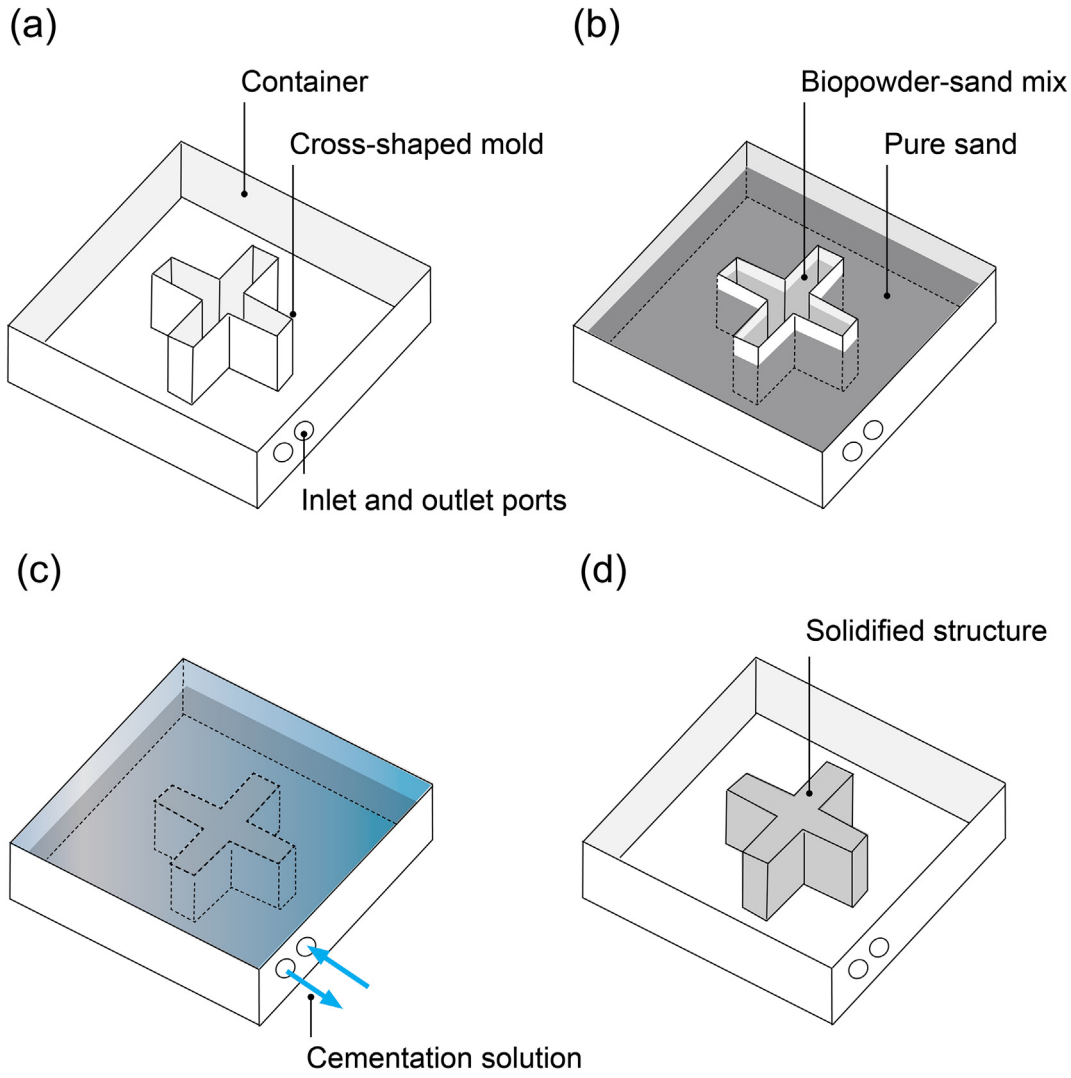

Fig. 5. Solidification of the urease active calcium carbonate powder-sand mix: (a) Container with inlet and outlet ports and the cross-shaped mold; (b) Mold filled with the powder-sand mix surrounded by pure sand; (c) Container with the powder-sand mix and pure sand with removed mold filled with the cementation solution; (d) Solidified structure after removing the non-cemented pure sand.

carbonate powder and various concentrations of the cementation solution. The production process of the cylinders is described in 2.4.1.

Cylinders with a powder content of 1.5% and 5% (*w*/w) treated with 750 mM cementation solution of $CaCl_2$ and urea demonstrated higher cementation depth and more homogeneous cementation at 4 °C compared to cylinders treated at 22 °C. The cementation depth of the cylinders with a powder content of 5% (*w*/w) was about 5 mm at 22 °C and about 15 mm at 4 °C. Although cylinders with a powder content of 1.5% (*w*/w) reached the maximum cementation depth of 30 mm both at 4 °C and at 22 °C, a more homogeneous cementation and glossier surface was observed at 4 °C.

The influence of the powder content (0.4% to 2.8% (*w*/w)) was studied with a 750 mM cementation solution of $CaCl_2$ and urea at 10 °C. The cementation depth decreased with an increasing powder content. The UCS could only be measured for cylinders that were cemented to a depth of at least 20 mm and that could sustain their shape after removing them from the syringe bodies. From 0.4% to 2.4% (w/w) the UCS increased with an increasing powder content (Fig. 8). The non-parallel upper and bottom surfaces could cause the deviation in the UCS measurement of the cylinder with the powder content of 2.8% (w/w).

The influence of the concentration of $CaCl_2$ and urea (500 mM, 750 mM and 1000 mM) in the cementation solution was studied with a powder content of 1.6% and 2.4% (w/w) at 10 °C. The results of this study were combined with the results from the experiment with varying powder content (Fig. 9). The UCS and the cementation depth increased with the increasing concentration of cementation solutions.

Bio-cemented cylindrical specimens produced with urease active calcium carbonate powder demonstrated an UCS of up to 23 MPa, which is comparable to low strength concrete (C16/20).

3.3. Initial experiments: Cementation of the urease active calcium carbonate powder-sand mix surrounded by pure sand

The principal feasibility of the approach of creating non-cementable channels was demonstrated by the cementation of the urease active calcium carbonate powder-sand mix in one volume with pure sand. Powder and sand were placed separately as described in 2.5. The experiment showed, that only powder-sand solidified after the treatment with cementation solution. Pure sand was easily removed by rinsing with water. The solidified structure was stable and had sharply defined boundaries (Fig. 10).

3.4. Additive manufacturing process

To enable customization and precise production of the bio-cemented structures, a 3D printing process has been developed. The 3D printer consisted of a print head moving in the horizontal plane

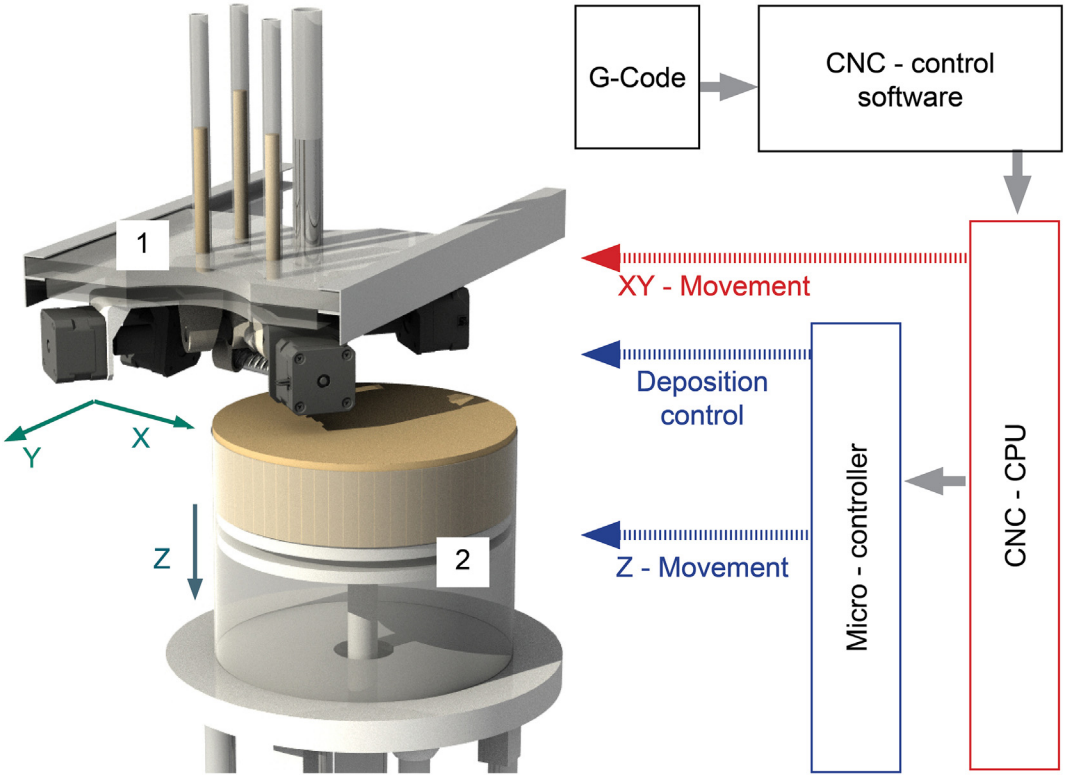

Fig. 6. Mechanical assembly of the 3D printer and the CNC-control scheme, where 1 - print head, 2 - print bed.

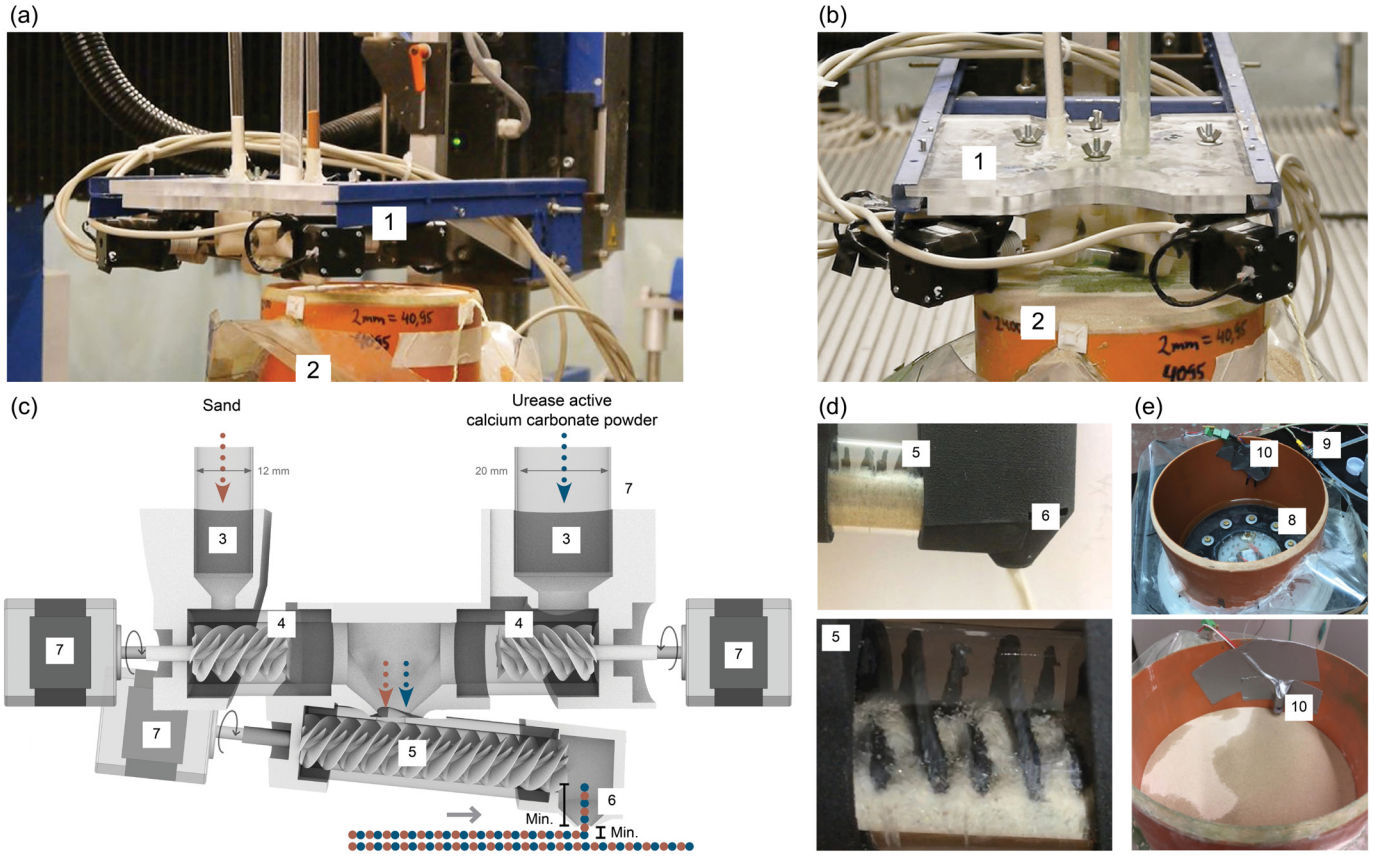

Fig. 7. 3D printer setup: (a) and (b) Pictures of the working 3D printer, where 1 - print head, 2 - print bed; (c) and (d) Material supply system of the print head, where 3 - vertical tubular glass reservoirs, 4 - feed screws, 5 - mixing screw, 6 - deposition nozzle, 7 - stepper motors; (e) Print bed, where 8 - platform pressed against the bottom plate and the gasket by fastening screws, 9 - solenoid valves, 10 - water sensor.

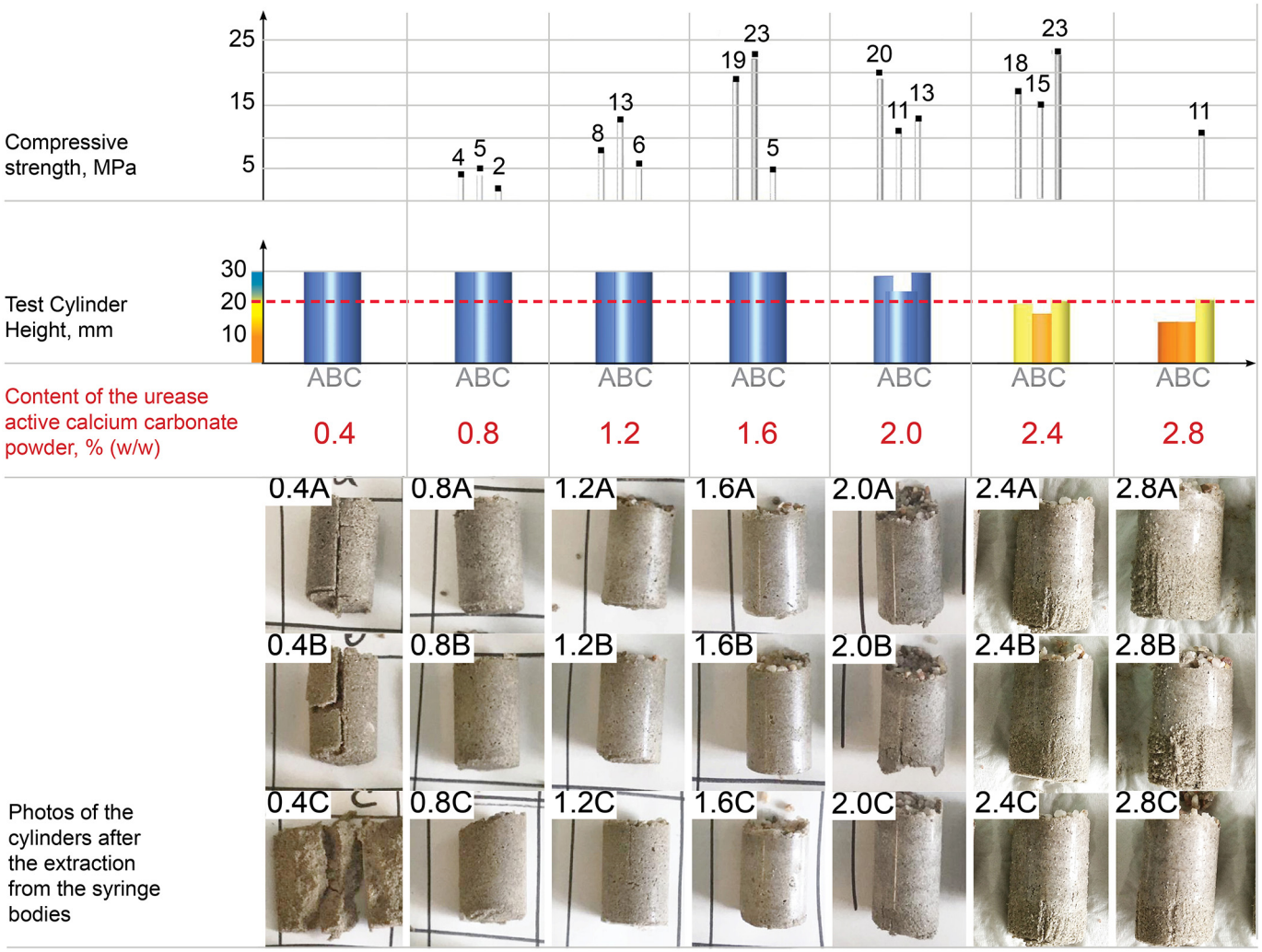

Fig. 8. Cylinders produced with contents of the urease active calcium carbonate powder ranging from 0.4% to 2.8% (*w*/w) and concentration of the cementation solution of 750 mM at 10 °C.

and a print bed with a platform moving in the vertical direction. The details on the mechanical assembly, flow control and cementation solution supply are described in 2.6.

3.4.1. Trajectory generation

The 3D model of the produced structure was designed in Rhino 5 (2015, Rhinoceros, Robert McNeel and Associates, USA).

The model of the porous strut structure had dimensions of 120 × 75 × 75 mm^3 with a solid volume of 347.6 cm^3 (Fig. 11 a). The strut thickness varied from 14 mm at the bottom to 7.5 mm at the top of the structure.

A custom C# script was used to slice the model volume into layers, generate trajectories of parallel lines for each layer, split them into segments located on the inside and the outside of the model volume (Fig. 11 b) and generate a G-code. For segments on the inside a powder-sand mix, whereas for those on the outside - pure sand, was to be deposited by the print head.

The layer height was set to 1.5 mm (80 layers in total) and the distance between the parallel trajectory lines within a layer to 4 mm.

Each layer was produced in two passes, depositing the powder-sand mix on the first pass and pure sand on the second. The trajectory generation strategy for the short sections included the backwards movement of the print head after depositing the powder-sand mix to empty the nozzle from the accumulated material.

3.4.2. Calibration

The amount of urease active calcium carbonate powder in the powder-sand mix was set to 40% (*v*/v) (ca. 13% (*w*/w)). The amount was increased compared to the tests on bio-cemented cylinders due to the lower density of the dry powder-sand mix. To achieve this ratio the feed screws were calibrated to dispense sand at 5.7 cm^3/min and powder at 2.3 cm^3/min. Due to the granular packing effect this resulted in a total volumetric flow of 6.0 cm^3/min. The pure sand without the powder was dispensed with the same volumetric flow. The movement speed of the print head was set to 1400 mm/min.

To achieve a color gradient, two feeding screws were used to dispense red and white sand in varying proportions whilst maintaining the total volumetric flow. One sand feeding screw was initially set to dispense red sand at 5.7 cm^3/min and the other to dispense white sand at 0 cm^3/min. This proportion was dynamically changed from layer to layer throughout the height of the structure resulting in rates of 5.7 cm^3/min for white and 0 cm^3/min for red sand for the last layer.

3.4.3. Printing process

The powder-sand mix (red and white sand in varying proportions) and pure sand (only red sand) were deposited layerwise by the print head on the platform of the print bed (Fig. 12). To accelerate the printing process the areas surrounding the structure were partially filled by hand. During the printing process a compaction of the deposited layers was observed, presumably caused by vibrations of the milling machine

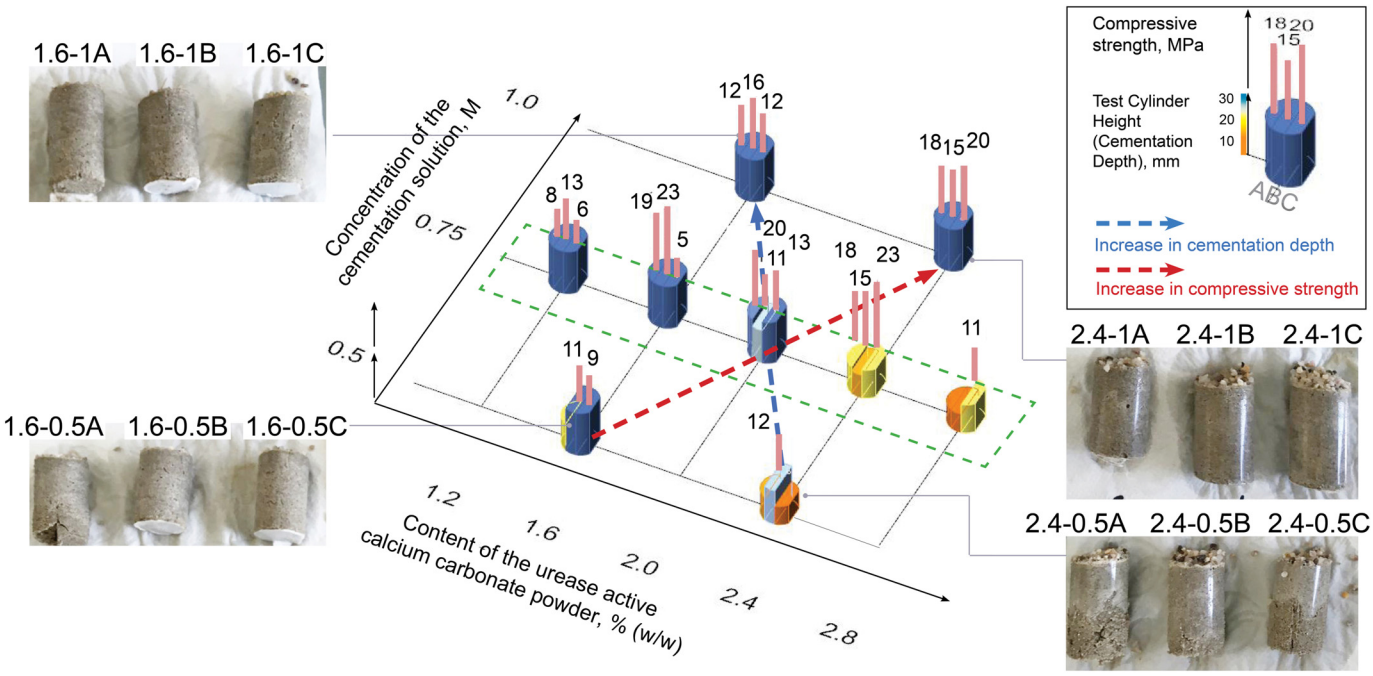

Fig. 9. Cylinders with contents of the urease active calcium carbonate powder of 1.6% and 2.4% (w/w) and concentration of the cementation solution of 0.5 M and 1 M at 10 °C (combined with the cylinders presented at Fig. 5 - marked with a green rectangle). (For interpretation of the references to color in this figure legend, the reader is referred to the web version of this article.)

Fig. 10. Cementation of the urease active calcium carbonate powder-sand mix surrounded by pure sand: (a) Non-solidified sand being removed revealing a solidified structure; (b) Solidified structure.

and the added load of the upper layers. After approximately 10 deposited layers the gap between the deposition nozzle and the previous layer was visibly larger than 1.5 mm and the platform had to be readjusted by reducing the downward movement for the following layer. The further the print progressed the more the compaction effect became visible, leading to more frequent readjustments of the platform.

3.4.4. Extraction of the printed structure

After the printing process was completed, the whole sand volume was treated with the cementation solution to start the biocementation. The cementation solution was supplied from a 50 cm elevated reservoir by opening the valve at the inlet port of the platform. After the water level reached the water sensor at the brim of the cylinder, the inlet valve was closed. After 5 min the outlet valve was opened to drain the cementation solution. This process was repeated 4 times at intervals of 8 h.

To retrieve the cemented structure after treatment, the print volume was rinsed with water to remove the uncemented sand. Afterwards, the structure was left to dry at room temperature for one week.

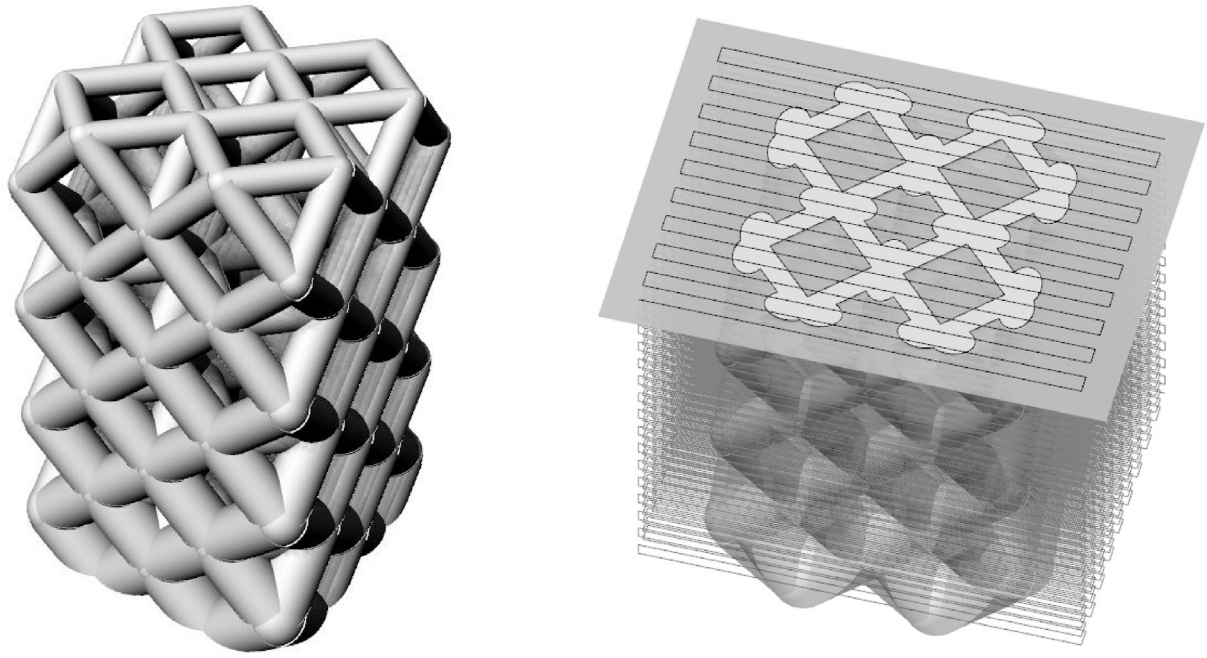

Fig. 11. 3D model of a printed structure: (a) Axonometric view; (b) Clipped view showing a print head trajectory within the layer.

3.4.5. Stability and geometrical accuracy of the printed structure

When extracting the 3D printed structure from the sand bed, the boundary between the cemented and the supporting sand was clearly distinguishable. The dried structure (Fig. 13 a) was cut vertically with a 1 mm thick abrasive cutting disc to examine its interior (Fig. 13 b). The structure was brittle at the top and displayed gradual increase in stability towards the bottom. This was reflected by the significant difference in effort needed to cut through the upper and through the lower quarters of the structure. Some supporting sand had not been washed out during rinsing with water and remained in the internal cavities of the structure. However, it was easily removed by scraping it off with a thin wooden stick.

Several dimensional measurements were taken and compared to the digital model to evaluate the geometrical accuracy of the 3D printed structure. The upper quarter, being partly destroyed, was excluded from the evaluation. The distance between the center points of the strut nodes were measured in the vertical and horizontal directions on the cut section of the structure (Fig. 14 a).

The comparison to the digital model (Table 2) showed that the 3D printed structure was increasingly compressed towards the bottom due to the compaction of sand and the readjustment of the print bed. In the horizontal direction almost no deviation was observed. The lower quarter of the structure was however shifted by 2 mm in Y-direction (printing direction) relative to the rest of the structure. This can be likely attributed to an unintended shift of the print bed while manually filling in the support material.

The strut thickness was measured separately on the side oriented parallel and on the side oriented perpendicular to the printing direction

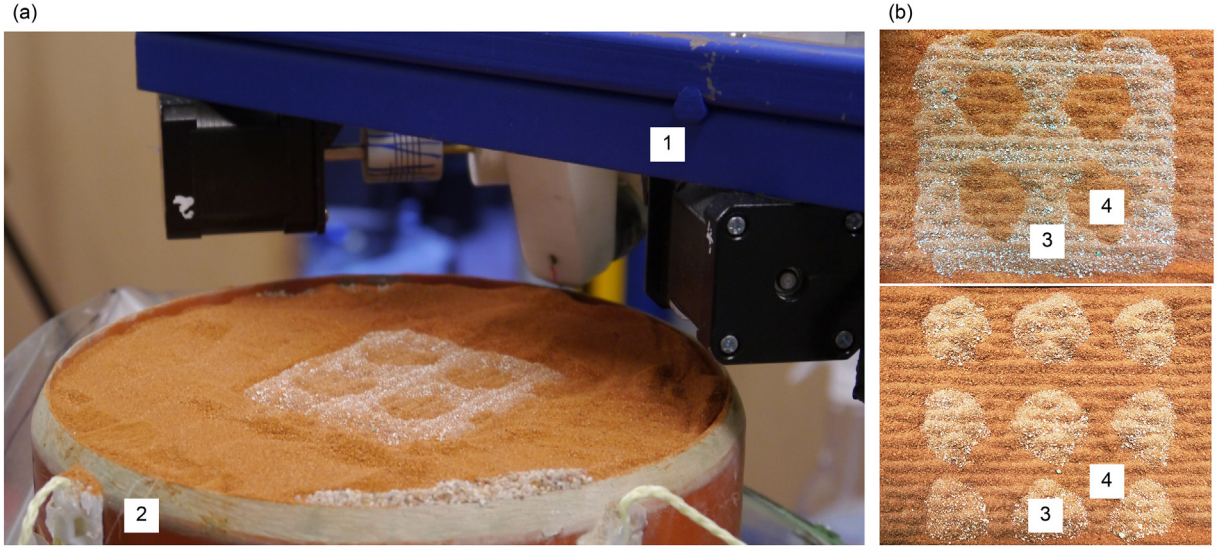

Fig. 12. 3D printing process: (a) Layer deposition by the print head - 1 on the print bed - 2; (b) Printed layers, where 3 – powder-sand mix (printed structure), 4 - pure sand (support structure).

Fig. 13. Spatial structure produced with the developed additive manufacturing method: (a) Before cutting; (b) After cutting.

(Fig. 14 b), (Table 3). The accuracy of the struts thickness decreased towards the top, especially on the side parallel to the printing direction.

This can be attributed to the resolution of the print head and the strategy of the trajectory generation for thin struts. The deviation on the side perpendicular to the printing direction can be caused by the resolution of the trajectory spacing of 4 mm.

4. Discussion

The spatial structure, produced in the present study, had sharply defined boundaries at its outer surface and its interior. Judging from the mechanical force that was needed to cut the structure and from the appearance of the mineralized material, no significant difference has been observed between the cementation degree of the inner and outer struts within one print level. This indicates that size limitations can be overcome when the cementation solution can penetrate deep into the structure through the non-cementable paths where no consumption of chemicals occurs. The clear boundary between the solidified structure and loose support material shows, that the urease active calcium carbonate powder facilitated the fixation of bacteria in sand.

The powder can be stored at low temperatures over extended periods of time with little decrease in urease activity (20% in six months as shown by the present study). Further investigations of the storage conditions are however necessary, for example long-term studies on the durability of the powder under different ambient conditions. Storage space requirements of the powder are minimal compared to bacterial suspensions.

The cementation depth and the mechanical strength of the specimens produced in this study were influenced by the amount of the powder, its urease activity and the concentration of the cementation solution. For a certain concentration increasing the amount of the powder resulted in a decrease of the cementation depth and UCS of the sample. However, when both the amount of powder and the concentration were increased, a deeper cementation and higher UCS were observed. This indicates the depletion of calcium ions and urea in the upper layers of the samples at lower concentration to powder content ratios. A further increase of the concentration in combination with high powder content could potentially lead to the formation of deeper cemented high-strength material, although clogging of the pore volumes might occur in this case.

Although cylindrical specimens cemented with urease active calcium carbonate powder-sand mix demonstrated an UCS comparable to low strength concrete (C16/20), the variation in UCS between samples produced with the same parameters requires further investigation of the cementation process.

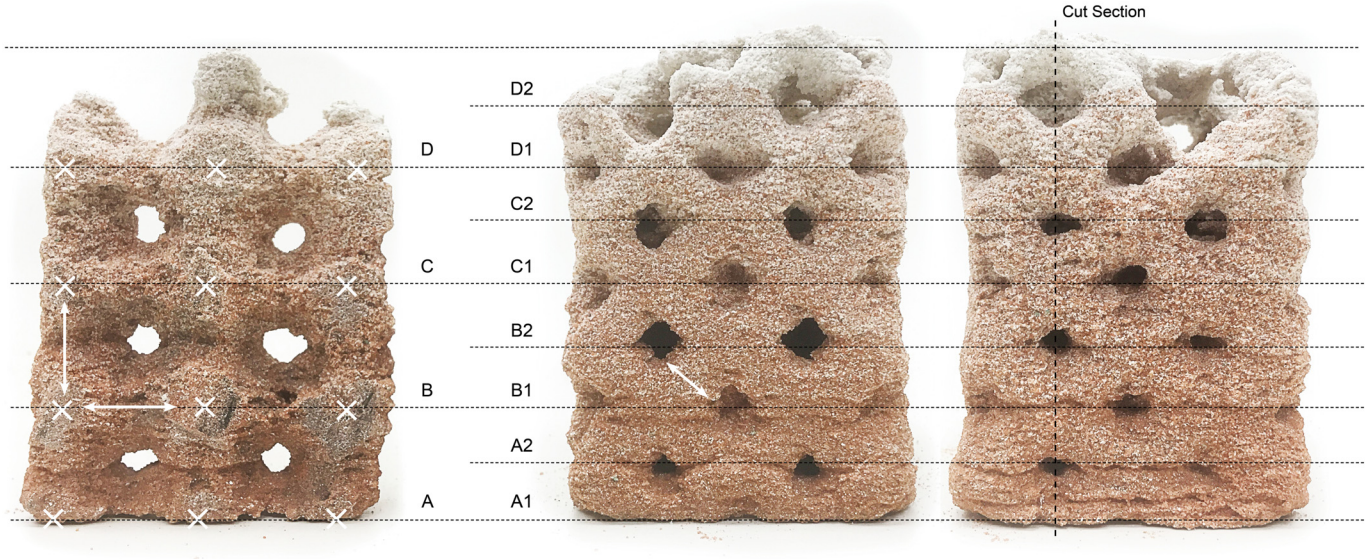

Fig. 14. Produced spatial structure: (a) The cut section with the marked center points of the strut nodes for the node distances evaluation; (b) Front view showing the segments for the strut thickness evaluation.

Table 2
Measurements of the distance between the nodes on the cut section of the structure.

Segment	Distance between the nodes in the vertical direction			Distance between the nodes in the horizontal direction		
	3D printed structure	Digital model	Deviation	3D printed structure	Digital model	Deviation
C–D	27.0 mm	30.0 mm	-10%	30.0 mm	30.0 mm	0%
B–C	26.0 mm	30.0 mm	-13%	30.0 mm	30.0 mm	0%
A–B	22.0 mm	30.0 mm	-27%	30.0 mm	30.0 mm	0%

The dry consistency of the powder-sand mix allows material placement with a high precision, that is only limited by the chosen grain size of the mix. The developed feed-screw system of the print head is not as fast and precise as other existing approaches for selective powder deposition like ultra-sonic powder dispensing [27] or dispensing with patterning drums [28]. However, these systems are designed to work with a small grain size range and therefore could not be implemented in the present work due to demixing of sand (largest grain size: 400 μm) and urease active calcium carbonate powder (smallest grain size: 1.3 μm) during dispensing. The precision of the developed method can be further improved by optimizing the printing trajectories and by reducing the nozzle diameter. Clogging of the nozzle could occur when the ratio between the nozzle diameter and the diameter of the largest particle is smaller than 5 [29]. In the present work this ratio was 11.25 and no clogging was observed. Larger nozzle diameters are preferable for the faster production, especially in the areas that only need to be filled with support material. Ideally a variable nozzle diameter could be implemented.

The dry powder-sand mix is less dense compared to a moisturized one and thus is subjected to compaction. The uneven compaction of sand led to a substantial decrease of accuracy in the vertical direction of the produced structure. Likely causes are the self-weight of the sand and vibrations from the movement of the CNC mill, as discussed in detail by Schmutzler et al. [30]. This inaccuracy needs to be either eliminated by developing compacting techniques to increase the bulk density of the mix or taken into account by creating digital and material models. The brittleness of the structure at the top could either have been caused by uneven and lighter compaction or by the rising cementation solution, which was supplied from the bottom and could have stirred up the upper sand layers. Both possibilities require further investigation.

Increasing the packing density of the mix would lead to a higher strength of the cemented material [31]. Furthermore, the reduction of the pore volume could facilitate faster cementation and reduce the total necessary amount of the urease active calcium carbonate powder and chemicals. Potentially a single treatment with cementation solution could be enough to reach a desirable strength of the produced material. In this case the two-step process of the mix deposition and the subsequent repeated treatment of the whole print volume could be simplified to a combined method, where the mix is deposited and immediately impregnated with cementation solution. This could lead to faster production times and there would be no need for non-cementable channels.

The industrial application of the presented production process is limited due to the size restriction of the print bed and the necessity of multiple print bed enclosures, as each enclosure would be occupied for the duration of the cementation process. Furthermore, the recovery of unused chemicals from the effluent cementation solution needs to be addressed in the future research.

Despite the high compressive strength, the tensile strength of the mineralized granular material is fairly low. Therefore, the incorporation of additional materials such as fibers [32] is necessary for the production of load-bearing building components. The addition of basalt fibers, that allow to achieve a fully mineral recyclable material, could be challenging due to the alkalinity of the cementation reaction that could damage the fibers [33].

Multimaterial 3D printing has the possibility to allow the variation of mix proportions. For example, by varying the amount of urease active calcium carbonate powder, gradients of bacterial activity can be created within a sample to further increase the homogeneity of cementation (similar to the effect of changing the activity by temperature [34]). The color gradient of the structure, produced in this study, was generated to express those potentials of the developed method.

Due to the necessity of non-cementable channels in the presented approach new typologies for porous structures must be developed for the successful implementation on a larger scale. This could be realized without loss in the load-bearing capacity through efficient material distribution within the component volume, as was demonstrated in the research field of functionally graded concrete [35]. In the context of the increasing resource scarcity the lightweight approach in a combination with the bio-concrete technology could contribute to the sustainable future of the building industry.

Credit authorship contribution statement

C. Nething and M. Smirnova: conceptualization, methodology, mechanical assembly, software, visualizations, experiments, writing – original draft, writing - review and editing of the paper; **J. A. D. Gröning:** preparation and urease activity measurements of the urease active calcium carbonate powder, writing - review and editing of the paper**; A. Stolz:** supervision of the laboratory experiments, resources, writing - review and editing of the paper; **W. Haase and W. Sobek:** supervision of the design research frame, resources, writing - review and editing of the paper.

Data availability

The processed data required to reproduce these findings are available to download from doi:10.17632/698cmpfkyn.1.

Table 3
Measurements of the strut thickness on the outer sides of the structure (average value for 2 surfaces).

Segment	Strut thickness - side perpendicular to the printing direction			Strut thickness - side parallel to the printing direction		
	3D printed structure	Digital model	Deviation	3D printed structure	Digital model	Deviation
D1	11.0 mm	7.7 mm	+ 43%	9.3 mm	7.7 mm	+ 20%
C2	11.3 mm	8.8 mm	+ 28%	10.5 mm	8.8 mm	+ 19%
C1	12.8 mm	9.9 mm	+ 26%	10.8 mm	9.9 mm	+ 9%
B2	13.0 mm	11.0 mm	+ 18%	10.8 mm	11.0 mm	- 2%
B1	15.0 mm	12.2 mm	+ 23%	12.8 mm	12.2 mm	+ 5%
A2	14.8 mm	13.3 mm	+ 11%	14.0 mm	13.3 mm	+ 5%

Declaration of Competing Interest

None.

Acknowledgment

This research received no external funding.

References

[1] R.M. Andrew, Global CO2 emissions from cement production, 1928–2018, Earth Syst. Sci. Data. 11 (2019) 1675–1710, https://doi.org/10.5194/essd-11-1675-2019.
[2] J.G.J. Olivier, J.A.H.W. Trends in global CO2 and Total Greenhouse Gas Emissions: 2019 Report, Netherlands Env. Asses. Agency, 12, 2019.
[3] V. Achal, A. Mukherjee, A review of microbial precipitation for sustainable construction, Constr. Build. Mater. 93 (2015) 1224–1235, https://doi.org/10.1016/j.conbuildmat.2015.04.051.
[4] M.J. Castro-Alonso, L.E. Montañez-Hernandez, M.A. Sanchez-Muñoz, M.R. Macias Franco, R. Narayanasamy, N. Balagurusamy, Microbially induced calcium carbonate precipitation (MICP) and its potential in bioconcrete: microbiological and molecular concepts, Front. Mater. 6 (2019)https://doi.org/10.3389/fmats.2019.00126.
[5] V. Achal, X. Pan, N. Özyurt, Improved strength and durability of fly ash-amended concrete by microbial calcite precipitation, Ecol. Eng. 37 (2011) 554–559, https://doi.org/10.1016/j.ecoleng.2010.11.009.
[6] D. Sarda, H.S. Choonia, D.D. Sarode, S.S. Lele, Biocalcification by Bacillus pasteurii urease: a novel application, J. Ind. Microbiol. Biotechnol. 36 (2009) 1111–1115, https://doi.org/10.1007/s10295-009-0581-4.
[7] D.J. Tobler, M.O. Cuthbert, R.B. Greswell, M.S. Riley, J.C. Renshaw, S. Handley-Sidhu, V.R. Phoenix, Comparison of rates of ureolysis between Sporosarcina pasteurii and an indigenous groundwater community under conditions required to precipitate large volumes of calcite, Geochim. Cosmochim. Acta 75 (2011) 3290–3301, https://doi.org/10.1016/j.gca.2011.03.023.
[8] V. Achal, A. Mukherjee, P.C. Basu, M.S. Reddy, Strain improvement of Sporosarcina pasteurii for enhanced urease and calcite production, J. Ind. Microbiol. Biotechnol. 36 (2009) 981–988, https://doi.org/10.1007/s10295-009-0578-z.
[9] L. Cheng, T. Kobayashi, M.A. Shahin, Microbially induced calcite precipitation for production of "bio-bricks" treated at partial saturation condition, Constr. Build. Mater. 231 (2020) 117095, https://doi.org/10.1016/j.conbuildmat.2019.117095.
[10] G.K. Dosier, Methods for Making Construction Materials Using Enzyme Producing Bacteria, US9199880B2, 2015.
[11] C. Bu, K. Wen, S. Liu, U. Ogbonnaya, Q. Dong, L. Li, F. Amini, Development of a rigid full-contact mold for preparing biobeams through microbial-induced calcite precipitation, Geotech. Test. J. 42 (2019) 20170148, https://doi.org/10.1520/GTJ20170148.
[12] D. Bernardi, J.T. DeJong, B.M. Montoya, B.C. Martinez, Bio-bricks: biologically cemented sandstone bricks, Constr. Build. Mater. 55 (2014) 462–469, https://doi.org/10.1016/j.conbuildmat.2014.01.019.
[13] S. Liu, K. Du, K. Wen, W. Huang, F. Amini, L. Li, Sandy soil improvement through microbially induced calcite precipitation (MICP) by immersion, JoVE J. Vis. Exp. (2019) e60059, https://doi.org/10.3791/60059.
[14] C. Bu, K. Wen, S. Liu, U. Ogbonnaya, L. Li, Development of bio-cemented constructional materials through microbial induced calcite precipitation, Mater. Struct. 51 (2018) 30, https://doi.org/10.1617/s11527-018-1157-4.
[15] L. Cheng, R. Cord-Ruwisch, Upscaling effects of soil improvement by microbially induced calcite precipitation by surface percolation, Geomicrobiol J. 31 (2014) 396–406, https://doi.org/10.1080/01490451.2013.836579.
[16] V.S. Whiffin, L.A. van Paassen, M.P. Harkes, Microbial carbonate precipitation as a soil improvement technique, Geomicrobiol J. 24 (2007) 417–423, https://doi.org/10.1080/01490450701436505.
[17] M.-J. Cui, J.-J. Zheng, R.-J. Zhang, H.-J. Lai, J. Zhang, Influence of cementation level on the strength behaviour of bio-cemented sand, Acta Geotech. 12 (2017) 971–986, https://doi.org/10.1007/s11440-017-0574-9.
[18] A.A. Qabany, K. Soga, Effect of chemical treatment used in MICP on engineering properties of cemented soils, Géotechnique. 63 (2013) 331–339, https://doi.org/10.1680/geot.SIP13.P.022.
[19] Q. Zhao, L. Li, C. Li, H. Zhang, F. Amini, A full contact flexible mold for preparing samples based on microbial-induced calcite precipitation technology, Geotech. Test. J. 37 (2014) 20130090, https://doi.org/10.1520/GTJ20130090.
[20] T.R. Ginn, B.D. Wood, K.E. Nelson, T.D. Scheibe, E.M. Murphy, T.P. Clement, Processes in microbial transport in the natural subsurface, Adv. Water Resour. 26 (2002).
[21] T. Ghosh, S. Bhaduri, C. Montemagno, A. Kumar, Sporosarcina pasteurii can form nanoscale calcium carbonate crystals on cell surface, PLoS One 14 (2019), e0210339. https://doi.org/10.1371/journal.pone.0210339.
[22] M.P. Harkes, L.A. van Paassen, J.L. Booster, V.S. Whiffin, M.C.M. van Loosdrecht, Fixation and distribution of bacterial activity in sand to induce carbonate precipitation for ground reinforcement, Ecol. Eng. 36 (2010) 112–117, https://doi.org/10.1016/j.ecoleng.2009.01.004.
[23] L. Cheng, R. Cord-Ruwisch, In situ soil cementation with ureolytic bacteria by surface percolation, Ecol. Eng. 42 (2012) 64–72, https://doi.org/10.1016/j.ecoleng.2012.01.013.
[24] L. Cheng, M.A. Shahin, Urease active bioslurry: a novel soil improvement approach based on microbially induced carbonate precipitation, Can. Geotech. J. Ed. Choice. 01 (2016) 1376–1385, https://doi.org/10.1139/cgj-2015-0635@cgj-ec.2015.01.issue-5.
[25] G.W. Black, N.L. Brown, J.J.B. Perry, P. David Randall, G. Turnbull, M. Zhang, A high-throughput screening method for determining the substrate scope of nitrilases, Chem. Commun. 51 (2015) 2660–2662, https://doi.org/10.1039/C4CC06021K.
[26] DIN EN 1926:2007-03, Natural Stone Test Methods - Determination of Uniaxial Compressive Strength; German version EN 1926:2006, Beuth Verlag GmbH2007 https://doi.org/10.31030/9832913.
[27] X. Zhang, C. Wei, Y.-H. Chueh, L. Li, An integrated dual ultrasonic selective powder dispensing platform for three-dimensional printing of multiple material metal/glass objects in selective laser melting, J. Manuf. Sci. Eng. 141 (2019) https://doi.org/10.1115/1.4041427.
[28] A. Bedoret, M. Hick, K. Eckes, Device and Method for Manipulating Particles, US20190240902A1, 2019.
[29] I. Zuriguel, A. Garcimartín, D. Maza, L.A. Pugnaloni, J.M. Pastor, Jamming during the discharge of granular matter from a silo, Phys. Rev. E 71 (2005), 051303. https://doi.org/10.1103/PhysRevE.71.051303.
[30] C. Schmutzler, C. Boeker, M.F. Zaeh, Investigation of deviations caused by powder compaction during 3D printing, Procedia CIRP. 57 (2016) 698–703, https://doi.org/10.1016/j.procir.2016.11.121.
[31] M. Schmidt, E. Fehling, Ultra-High-Performance Concrete: Research, Development and Application in Europe, 228, ACI Special Publication, 2005.
[32] Y. Xiao, X. He, T.M. Evans, A.W. Stuedlein, H. Liu, Unconfined compressive and splitting tensile strength of basalt fiber–reinforced biocemented sand, J. Geotech. Geoenviron. Eng. 145 (2019), 04019048. https://doi.org/10.1061/(ASCE)GT.1943-5606.0002108.
[33] B. Wei, H. Cao, S. Song, Tensile behavior contrast of basalt and glass fibers after chemical treatment, Mater. Des. 31 (2010) 4244–4250, https://doi.org/10.1016/j.matdes.2010.04.009.
[34] Y. Xiao, Y. Wang, C.S. Desai, X. Jiang, H. Liu, Strength and deformation responses of biocemented sands using a temperature-controlled method, Int. J. Geomech. 19 (2019), 04019120. https://doi.org/10.1061/(ASCE)GM.1943-5622.0001497.
[35] M. Herrmann, W. Sobek, Functionally graded concrete: numerical design methods and experimental tests of mass-optimized structural components, Struct. Concr. 18 (2017) 54–66, https://doi.org/10.1002/suco.201600011.